Topological dynamical quantum phase transition in a quantum skyrmion phase

Vipin Vijayan [1], L. Chotorlishvili,[2] A. Ernst,[3,4,*] S. S. P. Parkin,[3] M. I. Katsnelson,[5] and S. K. Mishra [1]

[1]*Department of Physics, Indian Institute of Technology (Banaras Hindu University), Varanasi 221005, India*
[2]*Department of Physics and Medical Engineering, Rzeszów University of Technology, 35-959 Rzeszów, Poland*
[3]*Max Planck Institute of Microstructure Physics, Weinberg 2, D-06120 Halle, Germany*
[4]*Institute for Theoretical Physics, Johannes Kepler University, Altenberger Straße 69, 4040 Linz, Austria*
[5]*Radboud University, Institute for Molecules and Materials, Heyendaalseweg 135, 6525AJ Nijmegen, Netherlands*

The quantum skyrmionic phase is modeled in a two-dimensional helical spin lattice. This topological skyrmionic phase retains its nature in a large parameter space before moving to a ferromagnetic phase. Next-nearest-neighbor interaction improves the stability and it also causes a shift of the topological phase in the parameter space. Nonanalytic behavior of the rate function observed, when the system which is initially in a quantum skyrmion phase is quenched to a trivial quantum ferromagnetic phase, indicates a dynamical quantum phase transition. Dynamical quantum phase transition is absent when the system initially in a skyrmion phase is quenched to a helical phase.

Progress made in the last decade in controlling matter at quantum levels has made access to real-time dynamics of closed quantum many-body systems realizable [1,2]. This progress lifted the border between experimentally feasible physical reality and model systems. Ultracold atoms in optical lattices and trapped ions are examples in which such dynamical phenomena were observed in real time. Today, we have full access to the real-time dynamics of quantum many-body and finite systems, either isolated or coupled to the Markovian or non-Markovian environment. The experiments with terahertz pulses in solids [3–6], high magnetic field pulse experiments [7], etc. are also developments in the recent past which can be aided by a theoretical understanding of dynamical properties of the corresponding quantum systems, especially the study of the evolution of the system after a sudden change in its parameter or a quantum quench. When we talk about changing the parameter of a system, the first thing that comes to mind is the term phase transition. Phase transitions are the points in the parameter space of a system around which a small change in the control parameter manifests a drastic change to its characteristics. In a classical/thermal phase transition, the thermal fluctuations cause the destruction of long-range ordering and facilitate the phase transition. But when we study the changes of the parameters at zero temperature or ground states the characteristics of the phase transition become purely quantum, because here the phase transition is facilitated by

quantum fluctuations instead of thermal fluctuations. Such phase transitions are known as quantum phase transitions. Equilibrium quantum phase transitions (EQPT) are studied extensively, but we have a lesser understanding of quantum systems out of equilibrium. In order to theoretically aid the experimental developments mentioned earlier, we need to understand the dynamical quantum phase transitions (DQPT). Recent experimental developments identified a signature of dynamical behavior after a quench in a Haldane-like system [8]. Experiments with trapped ions were able to directly observe DQPTs [9]. The theoretical inspiration for the DQPT can be extracted from the Lee-Yang theorem, Fisher zeros, and accompanying analysis. (For more details refer to Ref. [10]).

From Lee-Yang analysis [11,12] one can arrive at the conclusion that for a partition function of external fields (like magnetic field), which also depends on the temperature T as $Z(T)$, when zeros exist and have a positive real value then each of those roots corresponds to nonanalyticity in the free energy, i.e., phase transition. Fisher extended this analysis to considering partition functions with complex temperature z instead of T, $Z(z)$. When Fisher zeros of $Z(z)$ overlap with the real axis it produces nonanalyticities or phase transitions; however, no such overlaps is observed in the course of an EQPT. The real values of Fisher zeros correspond to a different kind of phase transition, namely, DQPT [10,13]. Using these analyses, the essence of DQPTs can be explained briefly as follows [14–17].

Short-lived nonequilibrium phase transitions accompanied with a nonanalytic behavior of physical quantities as a function of time are a characteristic feature of DQPTs [14]. To study this we utilize a quantity $\mathcal{G}$, the Loschmidt amplitude, as a function of time t, given as

$$\mathcal{G}(t) = \langle \psi_0 | e^{-i\hat{H}t} | \psi_0 \rangle. \quad (1)$$

In a sense, it plays the same role in the study of states out of equilibrium as the partition function $Z = Tr(e^{-\beta\hat{H}})$ in the

thermodynamic equilibrium case. Here $\hat{H}$ is the Hamiltonian of the system, β is the inverse temperature, and ψ_0 is the initial state of the system. Here Z can be seen as the kind of partition function considered by Lee and Yang(with inverse temperature in place of temperature, still the conclusions of the analysis holds). And in the exponent term of $\mathcal{G}(t)$, if we take (it) as the complex temperature, $\mathcal{G}$ behaves like the partition function of complex temperature considered by Fisher.

Another quantity of interest is the rate function of the return probability, Eq. (2) (hereinafter referred to as rate function), which is analogous to the thermodynamic free energy. As discussed earlier, during a phase transition the thermodynamic free energy, $F = -\frac{ln(Z)}{\beta}$, turns out to be a nonanalytic function of a control parameter. Based on the analogy we established so far, we expect to see a nonanalytic behavior on $\mathcal{L}$ when there is a DQPT, since it is a dynamical analog of thermodynamic free energy. The rate function is given as

$$\mathcal{L}(t) = -\lim_{N \to \infty} \frac{1}{N} \ln |\mathcal{G}(t)|^2, \qquad (2)$$

where N is the number of degrees of freedom of the system.

DQPT has been intensively studied during the last decade [13,18–22]. In the present work we are interested in the interplay between topology and DQPTs considering the quantum skyrmion [23]. The scientific community is still fascinated by topological states of matter even though it has been over four decades since the discovery of the quantum Hall state, the first discovered topological state [24]. Topologically distinct states or topological states are those states which are classified based on a certain invariant [25,26]. Such states are said to be identical when we can move from one state to another by applying continuous smooth deformations (deformations which do not close the bulk energy gap) without changing the value of the invariant [27]. When the system shows this kind of resistance to deformation we say that it is topologically protected. Conventional states, which are earlier believed to be the same, may become topologically distinct. We discover this only when the accompanying physical behavior is detected, like in the case of the quantum Hall effect.

In the past few decades, scientists discovered many topological materials and states like topological insulators [28,29], topological crystalline insulators [30,31], topological semimetals [32,33], etc. This classification is based on the behavior of the corresponding band Hamiltonians in the reciprocal state. There are also nontrivial topological objects determined by their characteristics in real space, such as various types of topological defects in condensed matter [34].

Magnetic skyrmions are among the most popular types of topological defects studied currently. Skyrmions are particular examples of solitons that can be informally defined as localized waves with a stable shape (for a more accurate definition and detailed discussion see, e.g., Ref. [35]). They are related to peculiar localized noncolinear magnetic textures within magnetic systems [36–38]. Skyrmions are promised to be potential information carriers for the next generation of spintronic devices [39]. New studies suggest macroscopic skyrmion qubits design suitable for quantum computing technology controlling the helicity and dynamics of the skyrmions

through electric fields [40]. These developments make the study of the dynamics of quantum skyrmions demanding.

The formation of magnetic order in spin systems depends on different factors and competing interactions. Formation of noncolinear magnetic textures is mainly fueled by competing nearest-neighbor ferromagnetic and next-nearest-neighbor antiferromagnetic or asymmetric exchange interactions, termed as Dzyaloshinskii-Moriya interaction (DMI). In most cases, the DMI is the dominant mechanism forming nonconventional magnetic textures [41–57].

Recently, the quantum analog of magnetic skyrmions has been suggested and studied [23,58,59]. However, contrary to the classical skyrmion, the quantum skyrmion is not topologically stable in a rigorous sense. Qualitatively, it is not protected with respect to the quantum tunneling to the topologically trivial vacuum state. At the same time, it presents a quantum spin state with quite a special character reminiscent of its topologically protected classical analog. Here we use the words "topological phase" for the case of quantum skyrmions in this, not completely rigorous but intuitively clear, sense. To better understand the nature of this state we studied its real-time dynamical properties.

Unlike skyrmions [48,58,60–62], helical magnetic textures do not possess a topological invariant and a topological protection. Any classification of two-dimensional (2D) helical phases is difficult, and even properties of quantum skyrmions are not well explored. Recent attempts to discover quantum skyrmions show a certain degree of success. Lohani *et al.* [58] and Gauyacq *et al.* [59] could identify magnetization patterns of a quantum skyrmion, but topological protection of skyrmion phase was not explored. Sotnikov *et al.* used a quantum scalar chirality to identify a topological protection [23]. Siegl *et al.,* using topological index and winding parameters, were able to identify a skyrmion phase and quantify its stability [63]. All these works could only find a skyrmionic phase in the ground state. In the present work, we investigate the stability of quantum skyrmions in higher excited levels as well.

An important question is the strength of the DMI. DMI can be determined in experiments or calculated accurately from first principles [64,65]. Our interest is focused on materials with large DMI [66–68]. In recent experimental works Yang *et al.* [69] has shown that magnetic films sandwiched between nonmagnetic layers exhibit DMI with an electrically tunable strength, i.e., **Co** films sandwiched between nonmagnetic layers or MgO/Fe/Pt. The value of DMI in such materials linearly increases with the applied external electric field $D = D_0 + g_{ME}E$, where D_0 is the intrinsic DMI part, g_{ME} is the magnetoelectric coupling, and E is the external electric field. Enhanced DMI can formally reach the order of exchange interaction for a large electric field. The dynamic control of intrinsic magnetic interactions by varying the strength of a high-frequency laser field allows further enhancing of the ratio between DMI and exchange interaction constants [61,70,71]. The idea relies on the fact that DMI and exchange interaction are both based on hopping processes and that time-periodic fields renormalize the electronic tunneling, leading to the effective rescaled DMI and exchange constants $D \approx \frac{4t\Delta}{U_0 - U}$ and $J \approx \frac{4t^2}{\Omega^2}(U_0 - U)$. Here Δ describes the Rashba spin-orbit
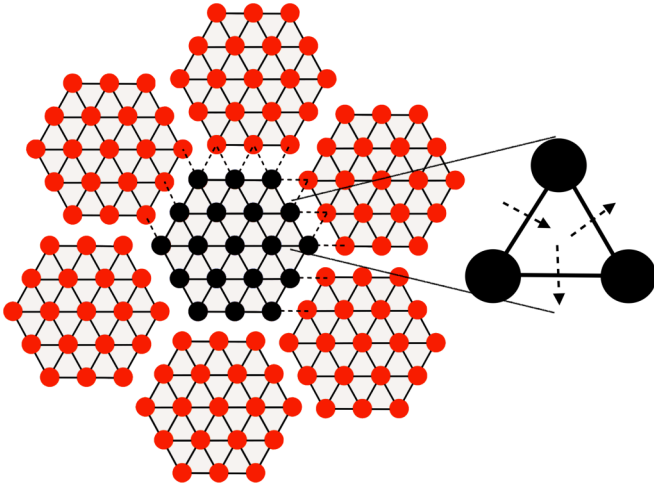
FIG. 1. PBC is applied to the 19 spins central supercell (black unit of the lattice). The supercell is repeated due to the PBC such that it forms a larger triangular lattice. The solid bonds show bonds within the boundary and the dashed bonds represent PBC. The bonds of this lattice can be classified into three based on their orientation. Hence, the direction of corresponding DMI vectors is also different for each of these categories of bonds. Three types of bonds and the direction of corresponding DMI vectors (dashed arrows) can be seen in the figure inset.
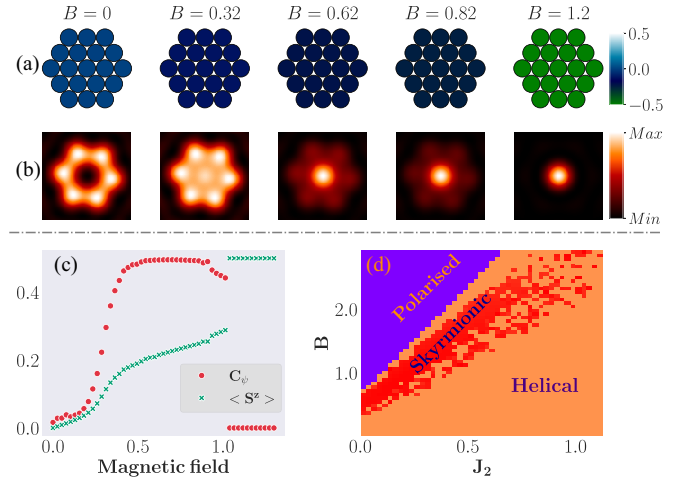

FIG. 2. (a) Locations of spins and spin textures of the local magnetization of a system at different values of an applied magnetic field. Here $D = 1$, $J_1 = -0.5D$, $J_2 = 0.1D$. The colors quantify expectation values of $\hat{S}_z$ components of specific spins. (b) The Fourier transform of the longitudinal spin correlation function for $D = 1$, $J_1 = -0.5D$, $J_2 = 0.1D$. The observed intensity peaks confirm the formation of nontrivial magnetic textures. (c) For $D = 1$, $J_1 = -0.5D$, $J_2 = 0.1D$, the quantum scalar chirality remains constant between magnetic field values of $0.46D$ and $0.86D$. (d) A phase diagram showing ferromagnetic, skyrmionic, and helical phases using the scalar chirality in the $J_2 - B$ parametric space.

coupling, t denotes the hopping amplitude, $U_0 - U$ is the gain in the Coulomb energy due to the electron displacement, and Ω is the frequency of the laser field. Because of the factor $1/\Omega^2$, the high-frequency laser field can substantially reduce the rescaled exchange constant to achieve the condition $D > J$. In order to study helical-skyrmionic-ferromagnetic phases, we consider an array of spins formed in a triangular lattice. The spins are arranged in such a way that it has a sixfold rotation symmetry (see Fig. 1); also, with periodic boundary conditions (PBC) it possesses translation symmetry. The Hamiltonian of the system has the form

$$\hat{H} = B \sum_i \hat{S}_i^z + J_1 \sum_{\langle i,j \rangle} \hat{S}_i \hat{S}_j + J_2 \sum_{\langle\langle i,j \rangle\rangle} \hat{S}_i \hat{S}_j$$
$$+ \sum_{i<j} \mathbf{D}_{i,j}[\hat{S}_i \times \hat{S}_j], \qquad (3)$$

where summation in single brackets is taken over the nearest neighbors and in double brackets over the next-nearest neighbors, B is an external magnetic field, and the DMI vector $\mathbf{D}$ is aligned perpendicular to the bond between lattice sites i and j, see inset of Fig. 1. The direction of DMI vectors is chosen to ensure that the sixfold rotation symmetry holds. We note that in helical multiferroic insulators, the parameter D is an effect of the magnetoelectric coupling g_{ME} with an external electric field E, i.e., $D = g_{ME}E$. Thus, the strength of the DMI term can be controlled externally [62]. Here we consider both J_1 (a ferromagnetic nearest-neighbor exchange) and J_2 (an antiferromagnetic next-nearest-neighbor exchange) interactions along with the DMI.

An array of spins read along with the above Hamiltonian with a specific parameter set forms a quantum skyrmion. The nearest-neighbor ferromagnetic J_1 term encourages colinear

spin orientation while the DMI term compels noncolinear spin texture. These two competing interactions form classical skyrmions stabilized by the applied magnetic field. Below we show that adding even the small next-nearest-neighbor antiferromagnetic Heisenberg term J_2 improves the stability of quantum skyrmion structures. In general, it is well known that the J_2 term leads to spin frustration and formation of antiferromagnetic classical skyrmions [72]. However, quantum skyrmion structures are quite specific as compared to classical skyrmions. In particular, quantum skyrmions do not possess continuous magnetic texture and topological charge. Therefore, to infer the quantum skyrmion state, we exploit another tool, such as scalar chirality. The energy levels of the system Eq. (3) show a sixfold degeneracy even at very high magnetic field values. We calculated the expectation values considering the maximally mixed state of these degenerate states with equal probability.

We used spin correlation functions to characterize quantum nontrivial magnetic structures. In particular, we explore the Fourier transform of the longitudinal spin correlation function $G_{\parallel}(\mathbf{q}) = \frac{1}{N} \sum_{ij} G_{\parallel}(\mathbf{r}_{ij}) \exp(-i\mathbf{q}\mathbf{r}_{ij})$, where N is the number of spins and the correlation function is given by

$$G_{\parallel}(\mathbf{r}_{ij}) = \frac{1}{Z} \sum_n \langle n|\hat{S}_i^z \hat{S}_j^z|n \rangle \exp(-\beta E_n), \qquad (4)$$

where E_ns are the eigenvalues of the Hamiltonian of the system and r_{ij} is the distance between the lattice sites i and j.

Topologically protected systems like skyrmions tend to show resistance to a deformation in its configuration [73,74]. Throughout this work an applied magnetic field is considered as a cause of deformation. In Figs. 2(a) and 2(b), panels are
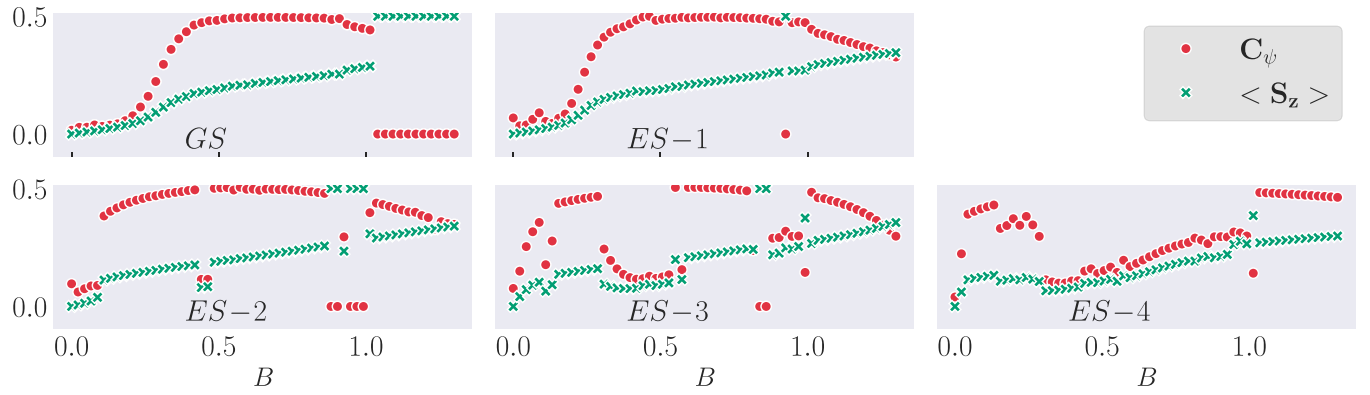
FIG. 3. Chirality and magnetization vs field for the first few eigenstates for $D = 1$, $J_1 = -0.5D$, $J_2 = 0.1D$. Here GS stands for the ground state and ES stands for exited states. In GS, ES-1, ES-2, and ES-3, we can identify the scalar chirality C_ψ with the almost constant value (at $C_\psi \sim 0.5$) corresponding to a certain range of the magnetic field B. For the GS the range of B is $B \sim 0.48D$ to $B \sim 0.91D$. In ES-1 it is $B \sim 0.48D$ to $B \sim 0.89D$. In ES-2 it is $B \sim 0.48D$ to $B \sim 0.85D$. In ES-3 it is $B \sim 0.59D$ to $B \sim 0.79D$. We notice that for higher excited energy levels the range of the plateau is diminished, and at ES-4 we completely lose the plateau. An important fact is that already for the first excited state ES-1, we observe fluctuation in the case of the strong field $B \sim 0.9D$. For higher excited states ES-2 and ES-3 fluctuations are enhanced and features of the quantum skyrmion state are absent.

arranged in the increasing order of applied magnetic field from left to right. Figure 2(a) shows that the local magnetization is uniform and increasing magnetic field causes the local magnetization to increase in the direction of the field. This observation fails to identify any magnetic textures in the system. In Fig. 2(b), multiple intensity spots (Bragg peaks) observed for nonzero **q** (Fourier conjugate of r or wave vector in reciprocal space) confirms the formation of quantum nontrivial magnetic texture [61]. This quantity could distinguish between helical and ferromagnetic phases but it fails to identify a skyrmionic phase within the helical phase. So, we require another quantifier that can trace out the skyrmion phase from helical and ferromagnetic phases.

Scalar chirality [23],

$$\mathbf{C}_\Psi = \frac{\mathcal{N}}{\pi} \langle \hat{S}_1 [\hat{S}_2 \times \hat{S}_3] \rangle, \tag{5}$$

is considered as a distinguishing property of a helical spin system. When the chirality has a nonzero value we say that the system is in a helical phase. It is proposed that chirality can distinguish quantum skyrmion phase from other phases of the system [23].

In this equation $\mathcal{N}$ is the number of nonoverlapping elementary triangular patches covering the lattice. Three adjacent spins form a patch. The scalar chirality for any of these three adjacent spin combinations is the same, because of the translational and rotational symmetries of the lattice.

In Fig. 2(c), from $B = 0D$ to $B = 0.46D$ chirality increases almost steadily. In this region no two deformed states have the same chirality value, therefore all those states are topologically nonidentical. From $B = 0.46D$ to $B = 0.86D$ the plateau of scalar chirality implies that all the states in this region have a common topological invariant, and we call them topologically identical phases or simply topological phases. After crossing $B = 0.86D$ the system briefly falls back to a helical phase. It is represented by a dip in chirality. Then around $B = 1.0D$ the system goes to the trivial ferromagnetic phase, indicated by zeros of scalar chirality.

In Fig. 2(c) the magnetization graph is telling us that for the region where we have a plateau in chirality the magnetization is not the same for any two states, i.e., the system is in fact undergoing deformation during the constant chirality plateau also.

The phase diagram [Fig. 2(d)] shows that for nonzero J_2 the invariance of scalar chirality extends for larger values of the applied magnetic field compared to $J_2 = 0$. The skyrmion phase is embedded into the helical phase. For a larger value of the interaction parameter J_2, the system retains the skyrmion phase for a longer range of applied magnetic field. We studied the scalar chirality not only in the ground state but also in several excited states. We see that the skyrmion state survives in the first and second excited states, and a certain degree of topological invariance can be seen in higher excited states as well, see Fig. 3. When $J_2 = 0D$ we arrive at the results from Sotnikov *et al.* [23]. For higher values of $J_2 (J_2 > 0.35D)$ the plateau gets distorted.

Here we show that important information about helical and quantum skyrmion phases can be obtained from the analyses of topological DQPTs. Namely, when quenching the system from a quantum skyrmion to a topologically trivial phase, we observe a characteristic signature of a DQPT as a nonanalyticity in the rate function. On the other hand, a quench between a skyrmion and a helix does not lead to a DQPT.

Let the system be prepared in the ground state $|\psi_0\rangle$ of the Hamiltonian $\hat{H}_0 = \hat{H}(\lambda_0)$. At $t = 0$ the parameter λ is quenched to a new value $\hat{H}(\lambda_f)$, and the initial wave function is evolved to a new state $|\psi(t)\rangle = e^{-i\hat{H}t}|\psi_0\rangle$ under this new Hamiltonian. In order to describe the DQPT we study the Loschmidt amplitude (return amplitude) and the rate function, in the thermodynamic limit [75–80].

Our primary interest concerns DQPTs between a quantum skyrmion phase and a trivial phase. The quench protocol applied on a topological phase to a trivial (skyrmion to ferromagnet) phase produced a nonanalytic behavior of the rate function with respect to time. The result is plotted in Fig. 4(a)
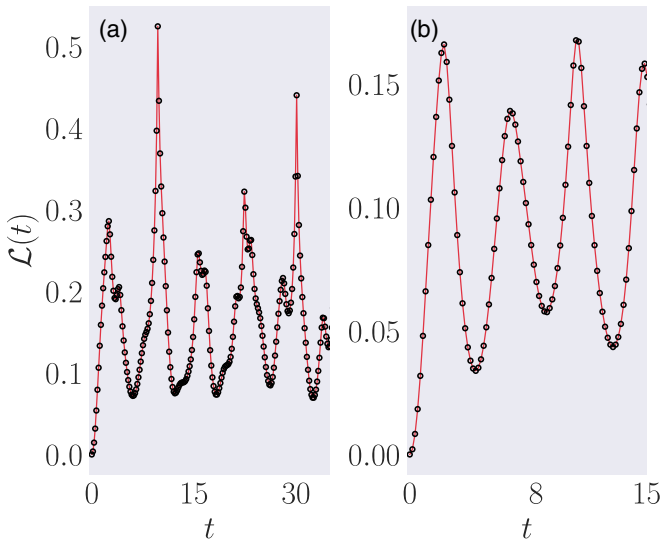
FIG. 4. Quench protocol is applied on ground state initiated with $D = 1$, $J_1 = -0.5D$, $J_2 = 0.1D$, $B = 0.85D$. (a) Time evolution of rate function for skyrmionic to polar phase transition. At $t = 0$ DMI is turned off (set $D = 0$). The peak of rate function at $t = 9.71$, 30.1, etc. shows nonanalytic behavior. (b) Time evolution of rate function for skyrmionic to helical phase transition. At $t = 0$ the applied field B is turned off. Here we do not find any nonanalyticity.

with respect to time: $L(t) \propto |t - t_c|^\alpha$, where α is the critical exponent. On the other hand, when switching between a skyrmionic phase to a helical phase, we do not observe any DQPT. We can confirm this from the lack of nonanalytic behavior of the rate function when plotted against time in Fig. 4(b). Here we looked for nonanalyticity with different values of the parameter B but we could not find any. The presence of nonanalyticity in the former case can be explained by a sharp and discontinuous transition of C_ψ from skyrmionic to trivial phase in Fig. 2(c). Similarly, the lack of nonanalyticity in the later case is due to the smooth and continuous transition of C_ψ from helical to skyrmionic phase. From Fig. 4(a) the critical exponent $\alpha = 0.7020 \pm 0.0233$ around $t_c = 9.66$. The value turned out to be very close to this for other critical points as well (see Supplemental Material for details [81], as well as Refs. [82–84] therein). Further study is required with larger system sizes [$L = 3i(i + 1) + 1$, $i = 3, 4, 5, ...$] in order to comment on the universality of the critical exponent that we calculated.

We have computational limitations to analyzing finite-size effects and artifacts of a particular quantum skyrmion state in our system. However, we performed the study of finite-size effects using another quantum skyrmion state obtained for a slightly different model in Ref. [63]. The results of the calculations are shown in Ref. [81]. We see the same trend for this case also, i.e., nonanalytic singularities in the rate function

during the dynamical quantum phase transition between the skyrmion and FM phases. Thus obtained results are pretty universal and apply to any quantum skyrmion. The reason for the universal effect is the orthogonality of quantum skyrmion and FM states. This argument is valid for any quantum skyrmion independent of its size.

Apart from this, we achieved a significant improvement of the topological phase stability with our model compared to the previous works [23,58,63]. We note that within a skyrmionic phase a larger J_2 value gives a topological phase protection against a larger range of applied magnetic fields. At high values of J_2 the topological invariance is destroyed. This result tells us that the key for tunability and improved stability of quantum skyrmions can be the interaction parameter, which may be useful when choosing the material to realize skyrmions for experiments. This kind of model is realized in the Pd/Fe/Ir(111) system with Co surrounded edges [85]. Also, nanoscale skyrmions are reported at room temperature with large DMI interaction in Ir/CoFeB/MgO systems [86].

In conclusion, the quantum skyrmion model proposed above shows significant improvement in topological protection. In said model we identified a robust DQPT when quench protocol is applied from a skyrmionic state to a ferromagnetic state. Robust DQPTs accompany many interesting properties. An interesting direction is to look for the connection between entanglement dynamics and DQPTs in a skyrmionic phase. Certain systems have reported to show an enhanced entanglement entropy around critical points of DQPTs [9].

[1] I. Bloch, J. Dalibard, and W. Zwerger, Rev. Mod. Phys. **80**, 885 (2008).

[2] I. Bloch, J. Dalibard, and S. Nascimbène, Nat. Phys. **8**, 267 (2012).

[3] B. Cole, J. Williams, B. King, M. Sherwin, and C. Stanley, Nature (London) **410**, 60 (2001).

[4] R. Huber, F. Tauser, A. Brodschelm, M. Bichler, G. Abstreiter, and A. Leitenstorfer, Nature (London) **414**, 286 (2001).

[5] R. A. Kaindl, M. A. Carnahan, D. Hägele, R. Lövenich, and D. S. Chemla, Nature (London) **423**, 734 (2003).

[6] S. Iwai, M. Ono, A. Maeda, H. Matsuzaki, H. Kishida, H. Okamoto, and Y. Tokura, Phys. Rev. Lett. **91**, 057401 (2003).

[7] F. Weickert, B. Meier, S. Zherlitsyn, T. Herrmannsdörfer, R. Daou, M. Nicklas, J. Haase, F. Steglich, and J. Wosnitza, Meas. Sci. Technol. **23**, 105001 (2012).

[8] N. Fläschner, D. Vogel, M. Tarnowski, B. S. Rem, D. S. Lühmann, M. Heyl, J. C. Budich, L. Mathey, K. Sengstock, and C. Weitenberg, Nat. Phys. **14**, 265 (2018).

[9] P. Jurcevic, H. Shen, P. Hauke, C. Maier, T. Brydges, C. Hempel, B. P. Lanyon, M. Heyl, R. Blatt, and C. F. Roos, Phys. Rev. Lett. **119**, 080501 (2017).

[10] A. Zvyagin, Low Temp. Phys. **42**, 971 (2016).

[11] C. N. Yang and T. D. Lee, Phys. Rev. **87**, 404 (1952).

[12] T. D. Lee and C. N. Yang, Phys. Rev. **87**, 410 (1952).

[13] M. Heyl, Rep. Prog. Phys. **81**, 054001 (2018).

[14] M. Heyl, A. Polkovnikov, and S. Kehrein, Phys. Rev. Lett. **110**, 135704 (2013).

[15] A. Deger, F. Brange, and C. Flindt, Phys. Rev. B **102**, 174418 (2020).

[16] R. Vosk and E. Altman, Phys. Rev. Lett. **112**, 217204 (2014).

[17] B. Gulácsi, M. Heyl, and B. Dóra, Phys. Rev. B **101**, 205135 (2020).

[18] T. H. Kyaw, V. M. Bastidas, J. Tangpanitanon, G. Romero, and L.-C. Kwek, Phys. Rev. A **101**, 012111 (2020).

[19] R. Jafari and A. Akbari, Phys. Rev. A **103**, 012204 (2021).

[20] M. Azimi, M. Sekania, S. K. Mishra, L. Chotorlishvili, Z. Toklikishvili, and J. Berakdar, Phys. Rev. B **94**, 064423 (2016).

[21] T. Masłowski and N. Sedlmayr, Phys. Rev. B **101**, 014301 (2020).

[22] T. Langen, R. Geiger, and J. Schmiedmayer, Annu. Rev. Condens. Matter Phys. **6**, 201 (2015).

[23] O. M. Sotnikov, V. V. Mazurenko, J. Colbois, F. Mila, M. I. Katsnelson, and E. A. Stepanov, Phys. Rev. B **103**, L060404 (2021).

[24] R. E. Prange and S. M. Girvin, *The Quantum Hall Effect*, 2nd ed. (Springer, New York, 1990).

[25] A. Altland and B. D. Simons, *Condensed Matter Field Theory*, 2nd ed. (Cambridge University Press, Cambridge, 2010).

[26] B. Zeng, X. Chen, D. Zhou, and X. Wen, *Quantum Information Meets Quantum Matter: From Quantum Entanglement to Topological Phases of Many-Body Systems*, Quantum Science and Technology (Springer, New York, 2019).

[27] X.-L. Qi and S.-C. Zhang, Rev. Mod. Phys. **83**, 1057 (2011).

[28] F. D. M. Haldane, Phys. Rev. Lett. **61**, 2015 (1988).

[29] M. Konig, S. Wiedmann, C. Brüne, A. Roth, H. Buhmann, L. W. Molenkamp, X.-L. Qi, and S.-C. Zhang, Science **318**, 766 (2007).

[30] T. H. Hsieh, H. Lin, J. Liu, W. Duan, A. Bansil, and L. Fu, Nat. Commun. **3**, 982 (2012).

[31] Y. Tanaka, Z. Ren, T. Sato, K. Nakayama, S. Souma, T. Takahashi, K. Segawa, and Y. Ando, Nat. Phys. **8**, 800 (2012).

[32] L. Fu and C. L. Kane, Phys. Rev. B **76**, 045302 (2007).

[33] F. Schindler, Z. Wang, M. G. Vergniory, A. M. Cook, A. Murani, S. Sengupta, A. Y. Kasumov, R. Deblock, S. Jeon, I. Drozdov, H. Bouchiat, S. Guéron, A. Yazdani, B. A. Bernevig, and T. Neupert, Nat. Phys. **14**, 918 (2018).

[34] N. D. Mermin, Rev. Mod. Phys. **51**, 591 (1979).

[35] R. Rajaraman, *Solitons and Instantons: An Introduction to Solitons and Instantons in Quantum Field Theory*, North-Holland personal library (North-Holland Publishing Company, Amsterdam, 1982).

[36] B. M. Piette, B. J. Schroers, and W. Zakrzewski, Z. Phys. C: Part. Fields **65**, 165 (1995).

[37] R. Rajaraman, in *Solitons and Instantons: An Introduction to Solitons and Instantons in Quantum Field Theory* (North-Holland, Amsterdam, 1982).

[38] T. H. R. Skyrme, in *Selected Papers, with Commentary, of Tony Hilton Royle Skyrme* (World Scientific, Singapore, 1994), pp. 195–206.

[39] A. N. Bogdanov and C. Panagopoulos, Nat. Rev. Phys. **2**, 492 (2020).

[40] C. Psaroudaki and C. Panagopoulos, Phys. Rev. Lett. **127**, 067201 (2021).

[41] A. A. Belavin and A. M. Polyakov, JETP Lett. **22**, 245 (1975).

[42] B. Barton-Singer, C. Ross, and B. J. Schroers, Commun. Math. Phys. **375**, 2259 (2020).

[43] B. J. Schroers, Phys. Lett. B **356**, 291 (1995).

[44] S. Seki, X. Yu, S. Ishiwata, and Y. Tokura, Science **336**, 198 (2012).

[45] M. N. Wilson, A. B. Butenko, A. N. Bogdanov, and T. L. Monchesky, Phys. Rev. B **89**, 094411 (2014).

[46] C. Schütte and M. Garst, Phys. Rev. B **90**, 094423 (2014).

[47] J. S. White, K. Prša, P. Huang, A. A. Omrani, I. Živković, M. Bartkowiak, H. Berger, A. Magrez, J. L. Gavilano, G. Nagy, J. Zang, and H. M. Rønnow , Phys. Rev. Lett. **113**, 107203 (2014).

[48] A. Derras-Chouk, E. M. Chudnovsky, and D. A. Garanin, Phys. Rev. B **98**, 024423 (2018).

[49] S. Haldar, S. von Malottki, S. Meyer, P. F. Bessarab, and S. Heinze, Phys. Rev. B **98**, 060413(R) (2018).

[50] A. Leonov and M. Mostovoy, Nat. Commun. **6**, 8275 (2015).

[51] C. Psaroudaki, S. Hoffman, J. Klinovaja, and D. Loss, Phys. Rev. X **7**, 041045 (2017).

[52] K. A. van Hoogdalem, Y. Tserkovnyak, and D. Loss, Phys. Rev. B **87**, 024402 (2013).

[53] S. Rohart, J. Miltat, and A. Thiaville, Phys. Rev. B **93**, 214412 (2016).

[54] A. Samoilenka and Y. Shnir, Phys. Rev. D **95**, 045002 (2017).

[55] R. A. Battye and M. Haberichter, Phys. Rev. D **88**, 125016 (2013).

[56] P. Jennings and T. Winyard, J. High Energy Phys. 01 (2014) 122.

[57] S. Tsesses, E. Ostrovsky, K. Cohen, B. Gjonaj, N. Lindner, and G. Bartal, Science **361**, 993 (2018).

[58] V. Lohani, C. Hickey, J. Masell, and A. Rosch, Phys. Rev. X **9**, 041063 (2019).

[59] J. P. Gauyacq and N. Lorente, J. Phys.: Condens. Matter **31**, 335001 (2019).

[60] H. Ochoa and Y. Tserkovnyak, Int. J. Mod. Phys. B **33**, 1930005 (2019).

[61] E. Stepanov, S. Nikolaev, C. Dutreix, M. Katsnelson, and V. Mazurenko, J. Phys.: Condens. Matter **31**, 17LT01 (2019).

[62] X.-G. Wang, L. Chotorlishvili, N. Arnold, V. K. Dugaev, I. Maznichenko, J. Barnaś, P. A. Buczek, S. S. P. Parkin, and A. Ernst, Phys. Rev. Lett. **125**, 227201 (2020).

[63] P. Siegl, E. Y. Vedmedenko, M. Stier, M. Thorwart, and T. Posske, Phys. Rev. Res. **4**, 023111 (2022).

[64] A. Fert, N. Reyren, and V. Cros, Nat. Rev. Mater. **2**, 17031 (2017).

[65] H. Yang, J. Liang, and Q. Cui, Nat. Rev. Phys. **5**, 43 (2023).

[66] P. Li, Q. Cui, Y. Ga, J. Liang, and H. Yang, Phys. Rev. B **106**, 024419 (2022).

[67] J. Liang, W. Wang, H. Du, A. Hallal, K. Garcia, M. Chshiev, A. Fert, and H. Yang, Phys. Rev. B **101**, 184401 (2020).

[68] Y. Zhang, C. Xu, P. Chen, Y. Nahas, S. Prokhorenko, and L. Bellaiche, Phys. Rev. B **102**, 241107(R) (2020).

[69] W. Zhang, H. Zhong, R. Zang, Y. Zhang, S. Yu, G. Han, G. L. Liu, S. S. Yan, S. Kang, and L. M. Mei, Appl. Phys. Lett. **113**, 122406 (2018).

[70] E. A. Stepanov, C. Dutreix, and M. I. Katsnelson, Phys. Rev. Lett. **118**, 157201 (2017).

[71] A. P. Itin and M. I. Katsnelson, Phys. Rev. Lett. **115**, 075301 (2015).

[72] T. Okubo, S. Chung, and H. Kawamura, Phys. Rev. Lett. **108**, 017206 (2012).

[73] S.-G. Je, H.-S. Han, S. K. Kim, S. A. Montoya, W. Chao, I.-S. Hong, E. E. Fullerton, K.-S. Lee, K.-J. Lee, M.-Y. Im *et al.*, ACS Nano **14**, 3251 (2020).

[74] H.-B. Braun, Adv. Phys. **61**, 1 (2012).

[75] M. Heyl, Phys. Rev. Lett. **113**, 205701 (2014).

[76] K. Brandner, V. F. Maisi, J. P. Pekola, J. P. Garrahan, and C. Flindt, Phys. Rev. Lett. **118**, 180601 (2017).

[77] J. Lang, B. Frank, and J. C. Halimeh, Phys. Rev. Lett. **121**, 130603 (2018).

[78] T. Tian, H.-X. Yang, L.-Y. Qiu, H.-Y. Liang, Y.-B. Yang, Y. Xu, and L.-M. Duan, Phys. Rev. Lett. **124**, 043001 (2020).

[79] X. Nie, B.-B. Wei, X. Chen, Z. Zhang, X. Zhao, C. Qiu, Y. Tian, Y. Ji, T. Xin, D. Lu, and J. Li, Phys. Rev. Lett. **124**, 250601 (2020).

[80] L. Pastori, S. Barbarino, and J. C. Budich, Phys. Rev. Res. **2**, 033259 (2020).

[81] See Supplemental Material at http://link.aps.org/supplemental/10.1103/PhysRevB.107.L100419 for detailed calculation of critical exponent α of dynamical Quantum phase transition when the system initially in quantum skyrmionic phase is quenched to a quantum ferromagnetic phase.

[82] D. Trapin, J. C. Halimeh, and M. Heyl, Phys. Rev. B **104**, 115159 (2021).

[83] M. Heyl, Phys. Rev. Lett. **115**, 140602 (2015).

[84] S. Bandyopadhyay, A. Polkovnikov, and A. Dutta, Phys. Rev. Lett. **126**, 200602 (2021).

[85] J. Spethmann, E. Y. Vedmedenko, R. Wiesendanger, A. Kubetzka, and K. von Bergmann, Commun. Phys. **5**, 19 (2022).

[86] R. Chen, X. Wang, H. Cheng, K.-J. Lee, D. Xiong, J.-Y. Kim, S. Li, H. Yang, H. Zhang, K. Cao, M. Kläui, S. Peng, X. Zhang, and W. Zhao, Cell Rep. Phys. Sci. **2**, 100618 (2021).